

Development of Interatomic Potential for Al-Tb Alloy by Deep Learning

Method

L. Tang¹, Z. J. Yang^{1,*}, T. Q. Wen², K. M. Ho^{2,3}, M. J. Kramer² and C. Z. Wang^{2,3,†}

¹*Department of Applied Physics, College of Science, Zhejiang University of Technology, Hangzhou, 310023, China*

²*Ames Laboratory-USDOE, Iowa State University, Ames, Iowa 50011, USA*

³*Department of Physics and Astronomy, Iowa State University, Ames, Iowa 50011, USA*

Corresponding author: * zejinyang@zjut.edu.cn † wangcz@ameslab.gov

Abstract

An interatomic potential for Al-Tb alloy around the composition of Al₉₀Tb₁₀ was developed using the deep learning method with DeePMD-kit package. The atomic configurations and the corresponding total potential energies and forces on each atom obtained in the *ab initio* molecular dynamics (AIMD) simulations are collected to train a deep neural network model to construct the interatomic potential for Al-Tb alloy. We show the obtained deep neural network model can well reproduce the energies and forces calculated by AIMD. MD simulations using the neural network interatomic potential also describe the structural and dynamical properties of Al₉₀Tb₁₀ liquid well, such as the partial pair correlation functions, the bond angle distribution, and the time dependence of mean-square displacement, in comparison with the results from AIMD. Furthermore, the developed neural network interatomic potential predicts the formation energies of crystalline phases of Al-Tb system with the same accuracy as *ab initio* calculations. The structure factor of Al₉₀Tb₁₀ metallic glass obtained by MD simulation using the developed neural network interatomic potential is also in good agreement with the experimental X-ray diffraction data.

I. Introduction

Aluminum-rare-earth (Al-RE) binary alloys with Al-rich composition (about 90 at. % Al) can form metallic glasses by rapid quenching from the liquid state [1]. It has been shown that these Al-rich Al-RE alloys have very high strength-to-weight ratio owing to a high proportion of light weight Al [2-4]. However, Al-RE alloys belong to marginal glass-forming alloys which usually have high density of nanocrystals in their solid samples [1, 5]. Moreover, the stable as well as metastable Al-based intermetallics vary across lanthanide series [1, 6-8].

In order to understand the microscopic mechanisms of phase formation and competition in these complex alloys, the knowledge of short to medium range orders in liquid and undercooled liquid at atomistic level and the corresponding time evolution of atomistic structure during solidification/devitrification of Al-RE alloys are critical. Investigation of the atomistic structural difference among these binary alloys will provide us an insight to further tune these alloys for better properties and glass-form ability.

We note that while most interest has been in the use of the light RE (e.g., Al-Ce [8]), the heavy RE have not been investigated as well, except for Al-Sm system at the composition around Al-90 atom% where both experimental studies and MD simulations using empirical interatomic potential have been reported [9-11]. By contrast, interatomic potentials and reliable structural analyses for the other Al-RE alloys (e.g., Al-Tb) are still lacking. Although *ab initio* calculations can offer high accuracy of interatomic interactions for all Al-RE alloys, it only deals with up to

hundreds of atoms with hundreds of picoseconds simulation time due to the limit of computational cost. Therefore, it is difficult for the *ab initio* calculation to investigate the long-time relaxation and other glass transition phenomena such as phase competition during solidification, which is a key to understand the metallic glass formation.

Recently, a deep learning method [12,13] with neural network model for many-body interatomic interactions has been developed and would satisfy both desirable accuracy and acceptable computational cost. This deep learning software package called DeePMD-kit [14] uses the total potential energies, forces on each atom, and virial for a set of atomic configurations from *ab initio* calculations as training data for machine learning. After the training process, the obtained deep neural network model is not only able to accurately reproduce the potential energies and forces of original training data set, but also accurately predicts structural and dynamical properties of the materials being modeled. This advantage makes the deep learning method suitable for studying solidification and devitrification of alloy systems because the new structural order may emerge during these phase transitions. Moreover, the interatomic potential from the trained deep neural network model can be used in standard LAMMPS package [15] to perform MD simulations. The computational cost of this MD simulations with deep neural network interatomic potential scales linearly with system size, which allows us to investigate the long range correlations and long-time relaxations in metallic glass systems.

In this paper, development of interatomic potential for Al-Tb Alloys by the deep

learning method is described. In order to enhance the sampling space, the training data set is comprised of liquid $\text{Al}_{90}\text{Tb}_{10}$, pure Al and Tb liquids, and various crystalline phases of pure Al, and pure Tb as well as Al-Tb binary compounds (see Table. 1). The potential energies and forces of training data set are calculated using VASP [16,17]. Then the accuracy of the obtained deep interatomic potential is tested by comparison the LAMMPS results with *ab initio* calculations and experiments.

The rest of paper is organized as follows. In Sec. II, we will present the detail of AIMD simulations to generate the data set for neural network model training. In Sec. III, we will show the parameters of deep learning process. In Sec. IV, we will demonstrate the reliability of obtained deep potential. Finally, summaries and conclusions are given in Sec. V.

II. Preparation of training data for deep potential learning

The training data set is critical for the success of the neural network machine learning to generate accurate interatomic potentials for reliable MD simulations of systems that we are interested in. The target of our deep neural network model is to simulate the liquid and glass structures of $\text{Al}_{90}\text{Tb}_{10}$ alloy. Hence, the training database is primarily composed of liquid $\text{Al}_{90}\text{Tb}_{10}$ at different temperatures. The $\text{Al}_{90}\text{Tb}_{10}$ liquid is simulated in a cubic cell with periodic boundary conditions containing 180 Al atoms and 20 Tb atoms. The size of unit cell is $15.989\text{\AA} \times 15.989\text{\AA} \times 15.989\text{\AA}$, which is according to the density of liquid Al (n_{Al}) and liquid Tb (n_{Tb}), i.e., $n_{\text{Al}_{90}\text{Tb}_{10}} = 0.9n_{\text{Al}} + 0.1n_{\text{Tb}}$. The time step of AIMD is taken as 3fs and NVT ensemble with Nose-Hoover

thermostat [18, 19] are used in all simulations.

First, we randomly collect the atomic structures of $\text{Al}_{90}\text{Sm}_{10}$ liquid in classic MD simulation as the initial configuration for the AIMD simulations and the simulation is performed at 2000K for 2000 MD steps. Next, the sample is quenched to 800K at a cooling rate of 3.3×10^{13} K/s. The atomic configurations at the temperatures of 2000K, 1800K, 1600K, 1400K, 1200K, 1100K, 1000K, 900K, 800K during the cooling process are taken as the initial structures of simulation for the following isothermal process. These initial configurations are relaxed isothermally for 90ps at the above nine different temperatures, respectively. Then, we randomly collected 240,000 snapshots (including the total potential energies, forces on each atom, and atomic configurations) from all the trajectories in the isothermal process of the AIMD simulations to train the deep potential model. At the same time, 30,000 different snapshots are collected as the validation data set for the deep potential model obtained from the neural network learning.

In experiment, phase separated fcc Al has been observed in the as-quenched Al-Tb glass [20]. In order to ensure that the deep potential can handle correctly possible phase separation, we also add the snapshots of the pure Al and Tb liquids/solids into the training data set. Both the pure liquid Al (Tb) and crystal fcc Al (hcp Tb) are calculated by VASP and included in the training data set. For the pure liquid Al, the sample is simulated isothermally at $T=1400\text{K}$ and 2000K while the simulation temperatures for liquid Tb is 1800K and 2200K , respectively. The AIMD simulations with initial configuration of Al (Tb) liquid containing 108 atoms are performed isothermally for

2000 steps to obtain the liquid state of Al (Tb). After that, the snapshots during the following 30ps simulations are collected for training data, where 18,000 snapshots for Al or Tb liquids respectively are randomly collected for the training set. In addition, another 2,000 snapshots of each pure liquids are collected for the validation data set.

The training and validation data set also included the information of the relevant crystalline phases. In order to obtain the snapshots of crystalline phases at finite temperature, AIMD simulations with a large supercell of fcc Al (hcp Tb) containing 108 atoms at $T=300\text{K}$ are employed. It allows the atoms to oscillate around the equilibrated positions in the crystals and then generate a serial snapshots of crystal structures with distortions. Moreover, in order to obtain the information about atomic structures and forces far from the equilibrium, we also carry out the *ab initio* simulations at different lattice constants. For fcc Al crystal the lattice constant is $a = 4.05(1 \pm 0.02n) \text{ \AA}$, $n = 0,1,2,3,4,5$. For hcp Tb crystal the lattice constant is $a = 3.60(1 \pm 0.02n) \text{ \AA}$, $c = 5.70(1 \pm 0.02n) \text{ \AA}$, $n = 0,1,2,3,4,5$. At each lattice constant, all atoms are distorted by means of AIMD simulations at $T=300\text{K}$. In these ways, we generate and randomly select 2,000 distorted fcc Al crystal structures and 2,000 distorted hcp Tb crystal structures at different lattice constants (or pressures) to be included in the training data set. Another 200 such distorted Al and Tb crystal structures respectively are also collected in the validation data set. In addition to the pure Al and Tb crystalline phases, we also include the known crystalline phases of Al-Tb alloy which covered the whole composition range, i.e., $\text{Al}_{17}\text{Tb}_2$ [21], Al_4Tb [22], Al_3Tb [23], Al_2Tb [24], AlTb [25], Al_2Tb_3 [26], Al_2Tb [27] and AlTb_3 [28], to the training data set.

For each of these crystalline phases, the snapshot structures were generated in the same way as that used for Al and Tb crystalline structures described above. Similarly, 2000 snapshot structures from AIMD simulations for each compound are included in the training data set and another 200 snapshots are used for the validation data set.

The overall information of training and validation data set are summarized in Table 1. All the energies and forces of the structures in the training and validation data sets are calculated by VASP package. The projector-augmented-wave (PAW) method [29] is used to describe the core-valence electron interaction. The generalized gradient approximation (GGA) in the Perdew–Burke–Ernzerhof (PBE) form [30] is used for the electronic exchange and correlation potential. The default energy cutoff for the plane wave basis set from PBE potential is used and only the gamma point is used to sample the Brillouin zone in all AIMD simulations.

III. Training the deep neural network model

In the present study, the Potential-Smooth version of DeePMD-kit software package [13] is used to train the deep neural network. It has demonstrated this deep learning method is very robust in developing interatomic potentials for MD simulation studies of liquid, crystalline bulk structures and organic molecules [13, 31]. The DeePMD-kit will learn how the potential energies and forces of an atom depended on its local environment within a cutoff radius. In this study, the radial cutoff is taken as 7.2 Å which is about the radial of second shell from the partial pair correlation function (PPCF) in AIMD simulations of Al₉₀Tb₁₀ liquid. The deep neural network model has

three hidden layers with equal numbers of nodes (240 nodes) per layer. The number of axis filter in the Potential-Smooth version of DeePMD is 4 and the filter network has two hidden layers with 50 and 100 nodes, respectively. The exponentially decaying learning rate is used and at the i th training step the learning rate is defined as $r_l(i) = 0.001 \times 0.96^{i/10000}$, where the start learning rate is 0.001 and the decay rate is 0.96 with decay step of 10000. In addition, the loss function is composed by root mean square (RMS) error of energy and force, while the virial term is not included because the information of virial is not used for training model. The prefactors of loss function on training process is able to change continuously from the initial training step to the last training step. For energy it starts at 0.2 and ends up to 2. Meanwhile, for forces the prefactor is 100 at beginning and goes down to 1 at the end of training process. The deep neural network is initialized with random numbers and the total number of training steps is 2,000,000.

IV. Performance of the deep potential

After the training process, the obtained deep neural network can reproduce the potential energies and forces of *ab initio* calculations, evidenced by the small RMS errors of energies and forces in comparison with the training data from *ab initio* calculations. Fig. 1(a) and (b) show the energy and force errors from 1000 snapshots of $\text{Al}_{90}\text{Tb}_{10}$ liquid which are randomly picked up from the validation data set and then compared the corresponding energies and forces between the DeePMD and *ab initio* calculations. The vertical coordinate represents the energies (forces) of those snapshots

calculated by the trained deep neural network while the horizontal coordinate is the corresponding energies (forces) obtained by *ab initio* calculations. It can be seen that the deep neural network can well reproduce the energies and forces for the given snapshots in the training data set. The RMS error is about 2.7 meV/atom for the energies and 0.11 eV/Å for the forces, which is sufficient for investigating the structures and dynamics of liquid. Moreover, the deep learning model can also well predict the energies and forces for the atomic configurations which has not been included in the training data set. For example, although the snapshots in the AIMD simulation at temperature 1300K is not in the training data set, Fig. 1(c) and (d) show excellent prediction of energies and forces of these atomic configurations. More details of the energy and force RMS errors from the deep model prediction for all the structures in the training data set are shown Table. 1. It can be seen that the obtained deep neural network can well reproduce all the training data including both liquid and crystalline structures.

The obtained deep potential can be used in MD package such as LAMMPS to study the temperature dependent structures and dynamics of liquid and glass. The comparison of PPCF between DeePMD and AIMD is one of the tests of the reliability of deep potential. Fig. 2 shows the total PPCF, Al-Al, Al-Tb, and Tb-Tb partial PPCFs of liquid $\text{Al}_{90}\text{Tb}_{10}$ at $T=2000\text{K}$ and 1300K calculated by AIMD and DeePMD. The initial configurations of both AIMD and DeePMD is the same and the simulation time for averaging PPCF is 30ps. It shows that the DeePMD can well reproduce the PPCFs of AIMD simulations even for the $\text{Al}_{90}\text{Tb}_{10}$ liquid sample at the temperature which is

different from that in the training data set. Note that the differences of Tb-Tb PPCF between AIMD and DeePMD can be attributed to the relatively poor statistics due to the small number of Tb atoms (only 20 atoms in a box) used in the simulation. In addition, the obtained deep potential can also well reproduce the PPCF of pure Al and Tb liquid, as shown in the Fig. 3.

Besides the PPCF, the bond angle distribution can provide more structure information about liquid sample. Thus, it can also be used to test the reliability of deep potential. For determining the bonding, we take the first minima of PPCF as the cutoff, i.e., if the distance of two atoms is smaller than the cutoff there is a bond connecting them. Moreover, all the snapshots for calculating PPCF are collected to do statistics of bonding angles. The angle distribution of bonds in the $\text{Al}_{90}\text{Tb}_{10}$ liquid at $T=1300\text{K}$ and 2000K are shown in Fig. 4 and 5, respectively. It can be seen that the deep potential can well reproduce the bonding angle distribution from *ab initio* calculations except the case of Tb-Tb-Tb bonds at $T=1300\text{K}$. This divergence may originate from the fact that there is a poor statistic owing to the small number of Tb atoms and the simulation time is much short (only 30ps).

The dynamics property of liquid, usually quantified by the mean-square displacement (MSD) as function of time, is also important for understanding the glass formability of metallic alloys. Fig. 6 shows the MSD as function of time for the atoms both in AIMD and DeePMD. It can be seen that the MSD curve has a good linear relationship with simulation time for both AIMD and DeePMD simulations, which is a typical dynamics character of liquid. As shown in Fig. 6, the slope of MSD obtained by

DeePMD is close to that of AIMD, indicating our obtained deep potential can well predict the self-diffusion coefficient. Again, it demonstrates the reliability of the obtained deep potential for Al₉₀Tb₁₀ alloy on the aspect of atomic dynamics properties.

Since glass formability strongly dependent on the competition with the nucleation and growth of various nearby crystalline phases, it is critical that the developed deep potential can describe well the energy landscape of the Al-Tb system at the composition of interest including possible stable and metastable crystalline phases. The competition among these crystalline phases and the glass formation upon the solidification would highly correlates with their formation energies. Here the obtained deep potential is used to calculate the formation energies of crystalline phases in Al-Tb system at T=0K. Pure fcc Al and pure hcp Tb were taken as the reference for calculating the formation energy. The formation energy is defined as $E_{\text{form}}(\text{Al}_m\text{Tb}_n) = [E(\text{Al}_m\text{Tb}_n) - nE(\text{Al}) - mE(\text{Tb})]/(n + m)$. Fig. 7 shows the comparison of formation energies between DeePMD and *ab initio* calculations. For the relaxation both in *ab initio* and DeePMD method, the conjugate gradient algorithm is used to obtain the optimized atomic structures. It can be seen that the formation energies of known stable crystalline phases in training data set predicted by DeePMD agree well with the results of *ab initio* calculations. Besides the crystal phases in the training data set, the obtained deep potential can also well predict the formation energies of crystal that is not included in the training data set. For example, we calculated the formation energies of other two types of Al₃Tb crystal (the hypothetical Al₃Tb with structure of Al₃Y [32, 33] and BaPb3-type Al₃Tb founded in ref. 23). The results show that the deep potential

reproduced the order of formation energy for all the three Al_3Tb phases although two of structures are not included in the training data set. Recently, it is found that several metastable crystalline phases are emerged in the devitrification process of $\text{Al}_{90}\text{Sm}_{10}$ system, which are identified by GA search [34, 35]. These structures of crystalline phases are valuable testing targets to see if the obtained deep potential still has ability of predicting the formation energies as well. We calculated the formation energies of $\text{Al}_{82}\text{Tb}_{10}$ (big tetra structure), $\text{Al}_{120}\text{Tb}_{22}$ (big cubic structure) and Al_5Tb (big hex structure) metastable phases in which the Al composition is close to 90%. As shown in Fig. 7, the formation energies produced by the deep potential are all close to the values of *ab initio* calculations. All the results of formation energies and relaxed lattice parameters obtained by DeePMD and *ab initio* calculations are listed in the Table. 2.

In addition to the comparison with *ab initio* calculations, we also perform MD simulations of Al-Tb liquid and glass using the developed deep learning potential to compare with the measurement from experiment. Experimentally, the liquid $\text{Al}_{91}\text{Tb}_9$ at 1174K was prepared by Cu-heart electric arc melting under Ar atmosphere and the glassy sample for $\text{Al}_{90}\text{Tb}_{10}$ was prepared by Cu block single melt-spinning technique, which are reported in ref. 20. The structure factors of the liquid and glass have been measured using high energy X-Ray diffraction (XRD) [20]. Our MD simulation of liquid $\text{Al}_{91}\text{Tb}_9$ is performed with 5000 atoms (4550 Al and 450 Tb) in a cubic box. The initial configuration is randomly picked up from the snapshots in previous MD simulation of liquid Al-Sm, where the Sm atoms are replaced by Tb atoms. First, the sample is equilibrated at 1174K for 30ps. Then MD trajectories in the subsequent

simulation of 30ps at the same temperature are collected to calculate $S(q)$. Fig. 8(a) shows the calculated and experimental total structure factor of $\text{Al}_{91}\text{Tb}_9$ liquid at $T=1174\text{K}$. As one can see in Fig. 8(a), the first and second peak of $S(q)$ from DeePMD agree well with the experimental data, except that there are some deviations around the first minimum. In addition, the height of pre-peak from DeePMD is higher than that of experimental data. The glass MD sample of $\text{Al}_{90}\text{Tb}_{10}$ (4500 Al and 500 Tb) at $T=300\text{K}$ is obtained by quenching from liquid of 2000K with cooling rate of 10^{11} K/s. One can see that the position and height of pre-peak from DeePMD at $T=300\text{K}$ well agrees with the experimental result, as shown in Fig. 8(b). Other peak positions and heights also agree well with experimental measurement. These results of comparison show that the MD simulation with our developed deep potential can reproduce the atomic structure in the experiment with sufficient accuracy.

V. Summary

In this paper, we have developed an interatomic potential of $\text{Al}_{90}\text{Tb}_{10}$ by DeePMD-kit software package based on neural network deep learning method. The VASP package is used to calculate the snapshots of liquid and crystal Al-Tb system for preparing the training data of machine learning. In order to train a transferable model, not only liquid $\text{Al}_{90}\text{Tb}_{10}$ but also the liquid of pure Al and pure Tb, as well as the crystalline structures of Al, Tb and binary Al-Tb compounds are included in the training data set for extending the sampling space. After the training process, the obtained deep neural network model has been demonstrated to predict well the energies and forces of

Al-Tb system for both configurations included and not included in the training data set.

The interatomic potential developed by the deep neural network model can be used in LAMMPS package to perform MD simulations. The results show that the deep potential can well predict the PPCFs and time-dependence of MSD of AIMD simulations. Moreover, the calculated formation energies of crystalline phases of Al-Tb system using the deep potential are found to be excellent agreement with *ab initio* results. Finally, the total structure factors calculated by deep potential agree well with the XRD data, especially the DeePMD can well reproduce the positions and heights of the peaks in structure factors of $\text{Al}_{91}\text{Tb}_9$ liquid and $\text{Al}_{90}\text{Tb}_{10}$ glass as those measured in experiment. The studies indicate that our developed interatomic potential of $\text{Al}_{90}\text{Tb}_{10}$ by deep learning method is reliable to simulate the atomic structure of $\text{Al}_{90}\text{Tb}_{10}$ alloy.

Acknowledgements

Work at Ames Laboratory was supported by the U.S. Department of Energy (DOE), Office of Science, Basic Energy Sciences, Materials Science and Engineering Division including a grant of computer time at the National Energy Research Supercomputing Center (NERSC) in Berkeley. Ames Laboratory is operated for the U.S. DOE by Iowa State University under contract # DE-AC02-07CH11358. L. Tang and Z. J. Yang acknowledge the support by the National Natural Science Foundation of China (Grant Nos. 11304279 and 11104247). Z. J. Yang also acknowledges the Natural Science Foundation of Zhejiang Province, China (Grant No. LY18E010007).

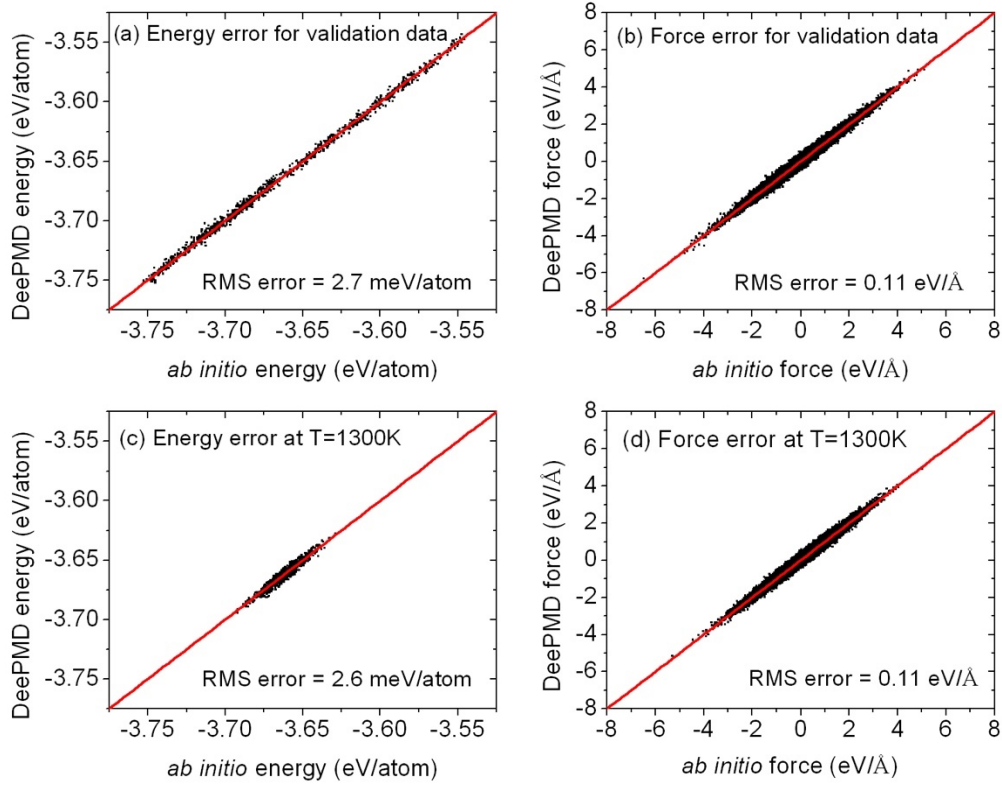


Fig. 1. Testing of energy and force prediction of the trained deep neural network model. In Fig. 1(a) and (b), the 1000 snapshots of $\text{Al}_{90}\text{Tb}_{10}$ liquid are randomly picked up from the validation data set to test the difference between DeePMD and *ab initio* results. In Fig. 1(c) and (d), the 1000 snapshots are collected from the AIMD simulation at $T=1300\text{K}$, where all the atomic configurations at this temperature are not included in training data set.

Systems in the training data set	Simulation temperatures (K)	Total simulation time (ps)	Total number of snapshots in training data set	Total number of snapshots in validation data set	Total number of atoms in box/supercell	Energy error (meV/atom)	Force error (eV/Å)
Al ₉₀ Tb ₁₀ liquid	2000, 1800, 1600, 1400, 1200, 1100, 1000, 900, 800	90 for each temperature	240,000	30,000	200	2.7	0.11
Tb liquid	1800, 2200	60	18,000	2,000	108	4.8	0.16
Tb crystal	300	6.6	2,000	200	108	4.4	0.09
Al liquid	1400, 2000	60	18,000	2,000	108	3.3	0.14
Al crystal	300	6.6	2,000	200	108	1.7	0.07
Al ₁₇ Tb ₂	300	6.6	2,000	200	304	3.0	0.08
Al ₄ Tb	300	6.6	2,000	200	120	1.9	0.08
Al ₃ Tb	300	6.6	2,000	200	240	1.4	0.08
Al ₂ Tb	300	6.6	2,000	200	192	1.0	0.08
AlTb	300	6.6	2,000	200	64	3.0	0.10
Al ₂ Tb ₃	300	6.6	2,000	200	160	2.1	0.09
AlTb ₂	300	6.6	2,000	200	216	2.5	0.10
AlTb ₃	300	6.6	2,000	200	108	2.8	0.09

Table 1. The overall information of training and validation data set for Al-Tb system. The RMS errors of the DeePMD energy and force prediction for the validation data set of various Al-Tb system are also shown in the table.

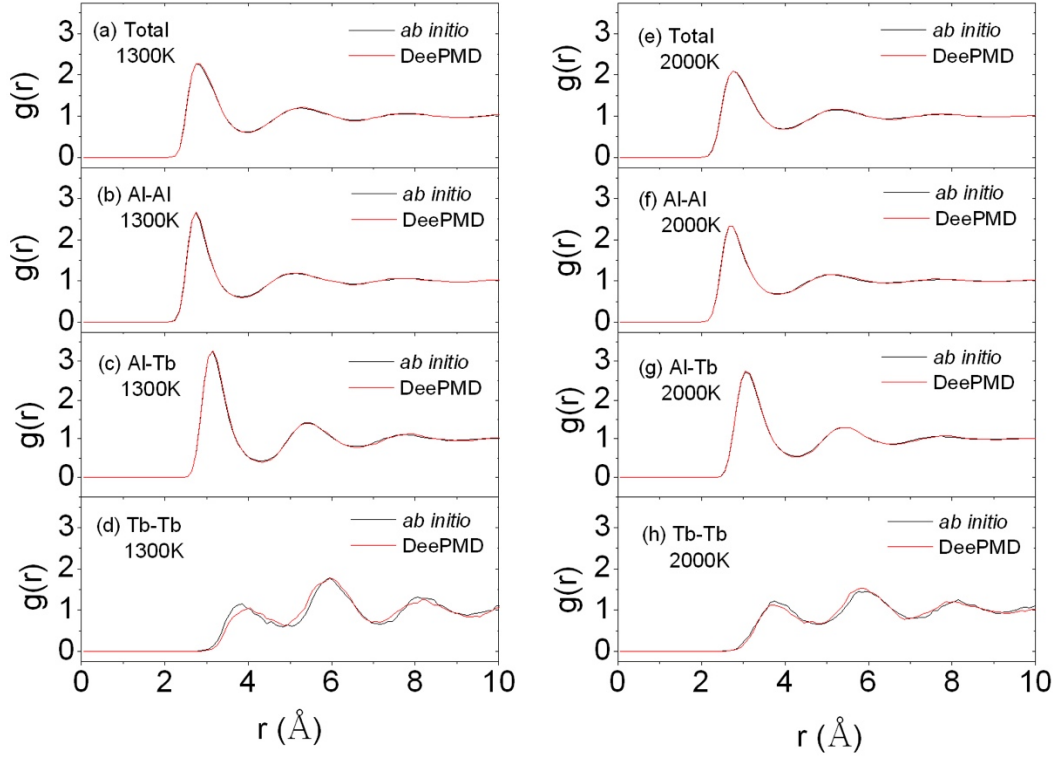


Fig. 2. Partial pair correlation functions in DeePMD and *ab initio* simulations for liquid $\text{Al}_{90}\text{Tb}_{10}$ at (a-d) $T=1300\text{K}$ and (e-h) 2000K .

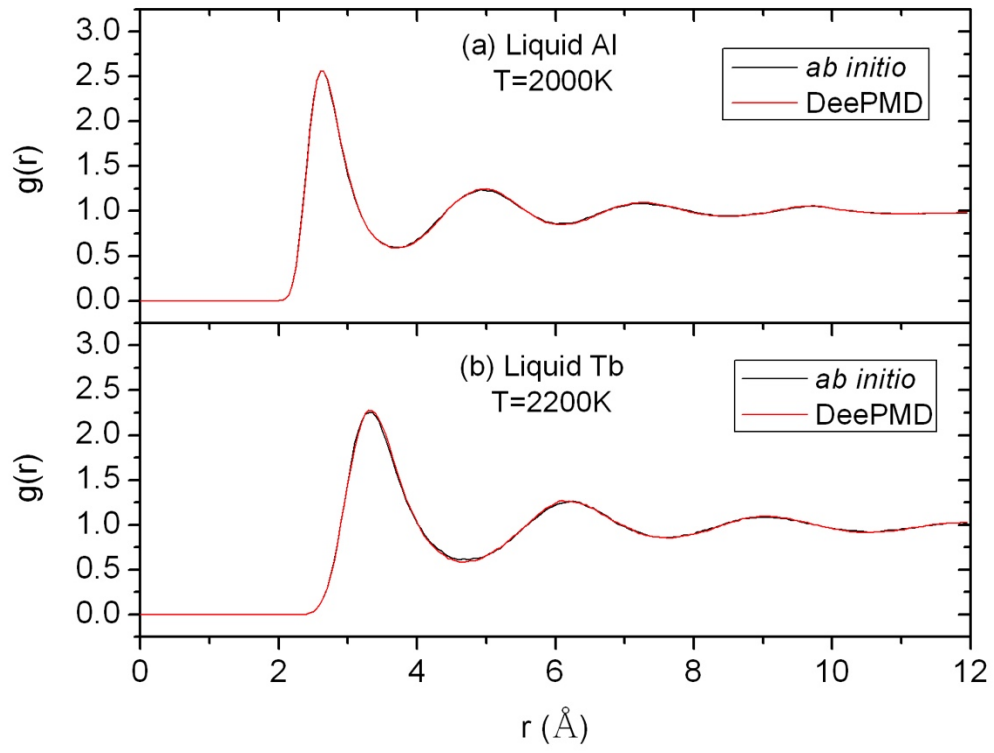


Fig. 3. Pair correlation functions in DeePMD and *ab initio* simulations for pure liquid (a) Al and (b) Tb.

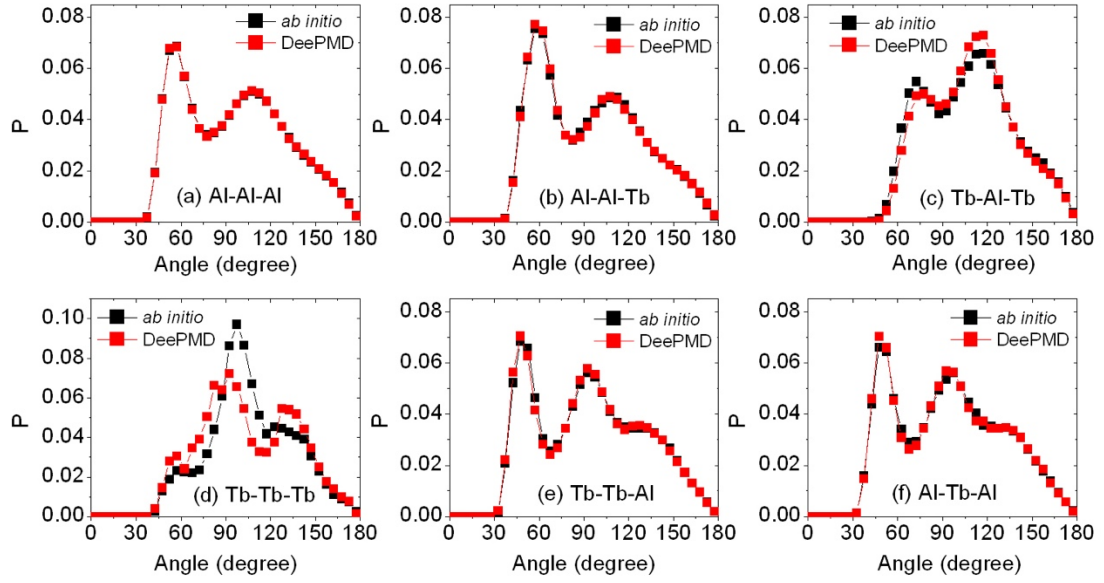


Fig. 4. The bond angle distribution in the liquid $\text{Al}_{90}\text{Tb}_{10}$ at $T=1300\text{K}$ from *ab initio* and DeePMD simulations.

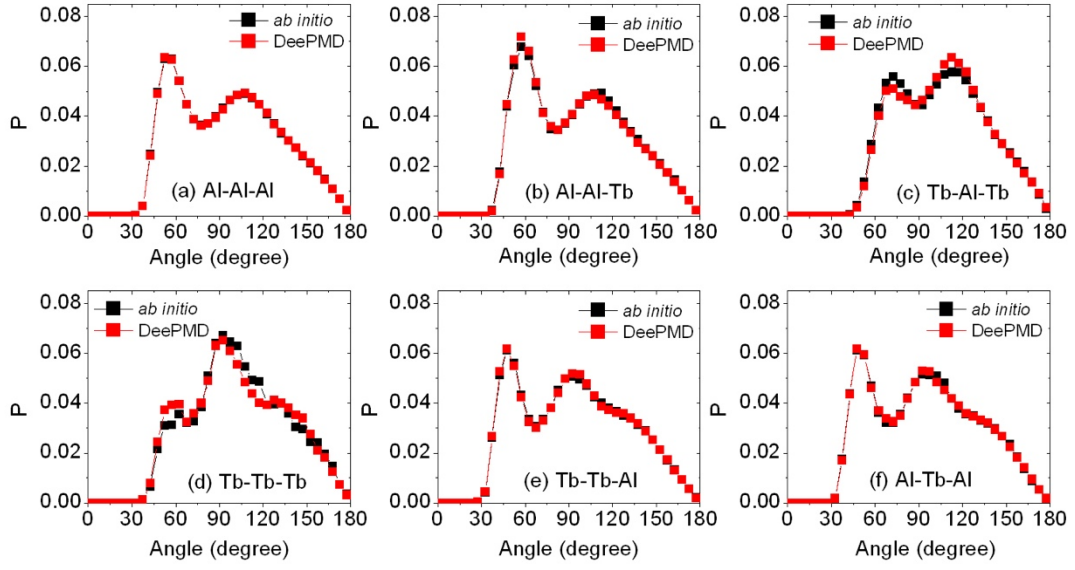


Fig. 5. The bond angle distribution in the liquid $\text{Al}_{90}\text{Tb}_{10}$ at $T=2000\text{K}$ from *ab initio* and DeePMD simulations.

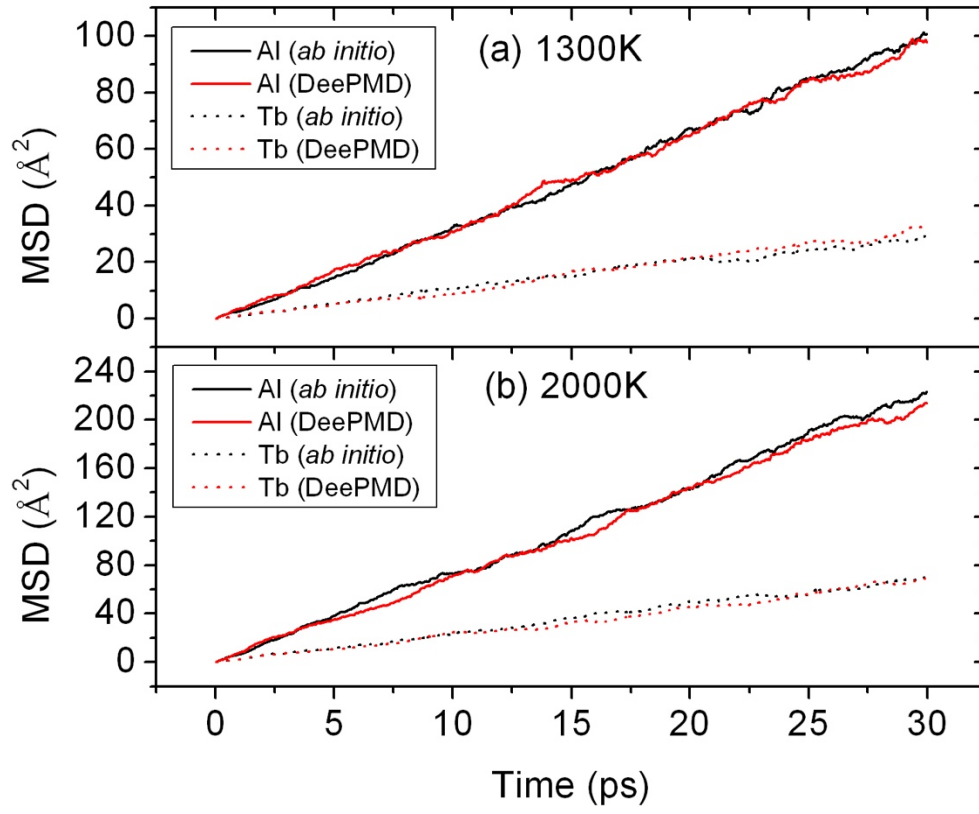


Fig. 6. The time dependence of mean square displacement of Al and Tb atoms in DeePMD and *ab initio* simulations at (a) $T=1300\text{K}$ and (b) 2000K .

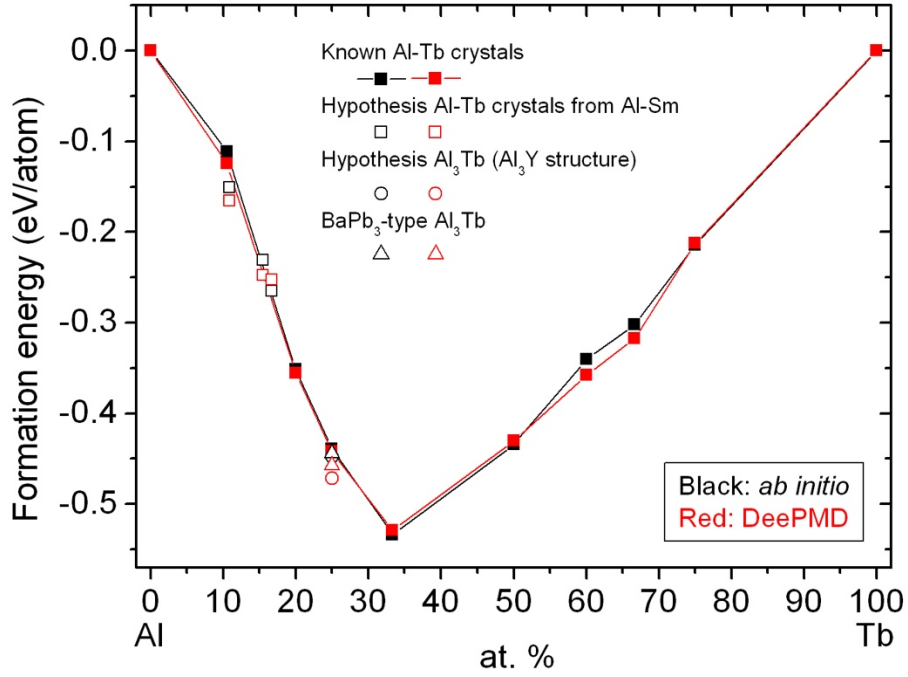
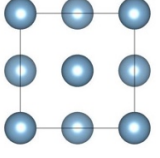
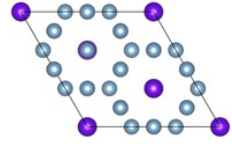
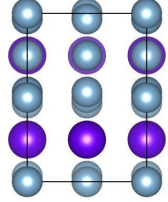
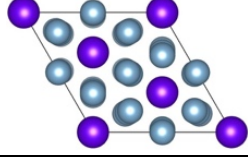
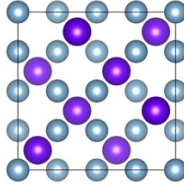
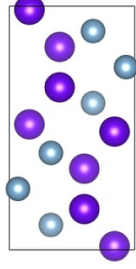
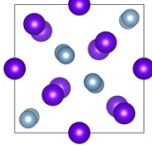
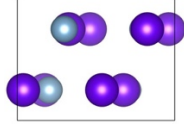


Fig. 7. The formation energies of Al-Tb system calculated by DeePMD and *ab initio* method at $T=0K$. The solid squares denote the known stable crystal structures in the training data set of Al-Tb system. The open squares denote the hypothesis Al-Tb crystal with the structures of metastable crystalline phases found in Al-Sm system. They are, from left to right, $Al_{82}Tb_{10}$ (big tetra structure), $Al_{120}Tb_{22}$ (big cubic structure), Al_5Tb (big hex structure). The open circles and triangles denote the hypothetical Al_3Tb with structure of Al_3Y and the BaPb₃-type Al_3Tb crystal, respectively. Noted that the open data is not included in the training data set, which suggests that the obtained deep potential has ability to predict the formation energy for the unknown Al-Tb structure around composition of 10% Tb.

crystalline phase	Structure	a (Å)	b (Å)	c (Å)	α (°)	β (°)	γ (°)	Formation energy (eV/atom)
Al		4.053	4.053	4.053	90	90	90	0
		4.038	4.038	4.038	90	90	90	0
Al ₁₇ Tb ₂		9.582	9.582	8.728	90	90	120	-0.124
		9.423	9.423	9.003	90	90	120	-0.112
Al ₄ Tb		4.463	6.308	13.808	90	90	90	-0.356
		4.415	6.295	13.785	90	90	90	-0.352
Al ₃ Tb		6.110	6.110	36.049	90	90	120	-0.442
		6.130	6.130	35.985	90	90	120	-0.439
Al ₂ Tb		7.920	7.920	7.920	90	90	90	-0.529
		7.888	7.888	7.888	90	90	90	-0.534
AlTb		5.873	11.454	5.661	90	90	90	-0.430
		5.861	11.476	5.638	90	90	90	-0.434
Al ₂ Tb ₃		8.297	8.297	7.607	90	90	90	-0.358
		8.276	8.276	7.615	90	90	90	-0.341
AlTb ₂		6.597	5.117	9.447	90	90	90	-0.318
		6.575	5.037	9.640	90	90	90	-0.302

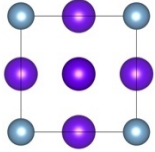
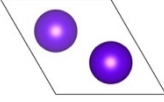
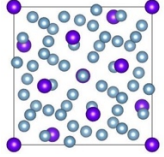
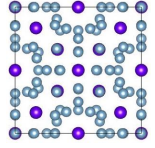
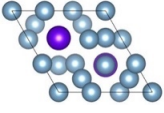
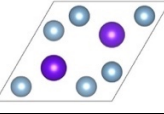
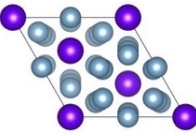
AlTb ₃		4.762	4.762	4.762	90	90	90	-0.212
		4.774	4.774	4.774	90	90	90	-0.214
Tb		3.605	3.605	5.706	90	90	120	0
		3.617	3.617	5.668	90	90	120	0
Al ₈₂ Tb ₁₀ (big tetra)		13.202	13.202	9.502	90	90	90	-0.165
		13.247	13.247	9.512	90	90	90	-0.151
Al ₁₂₀ Tb ₂₂ (big cubic)		13.781	13.781	13.781	90	90	90	-0.248
		13.822	13.822	13.822	90	90	90	-0.231
Al ₅ Tb (big hex)		5.407	5.407	17.729	90	90	120	-0.253
		5.430	5.430	17.636	90	90	120	-0.265
Al ₃ Tb (Al ₃ Y structure)		6.250	6.250	4.587	90	90	120	-0.472
		6.300	6.300	4.618	90	90	120	-0.448
BaPb ₃ -type Al ₃ Tb (from ref. 23)		6.175	6.175	21.172	90	90	120	-0.458
		6.208	6.208	21.187	90	90	120	-0.444

Table. 2. Lattice parameters and formation energies of Al-Tb crystalline phases. In calculation of the formation energy, fcc Al and hcp Tb crystal were taken as the reference states. The top value is reproduced by the DeePMD and the bottom one is calculated by the *ab initio* method.

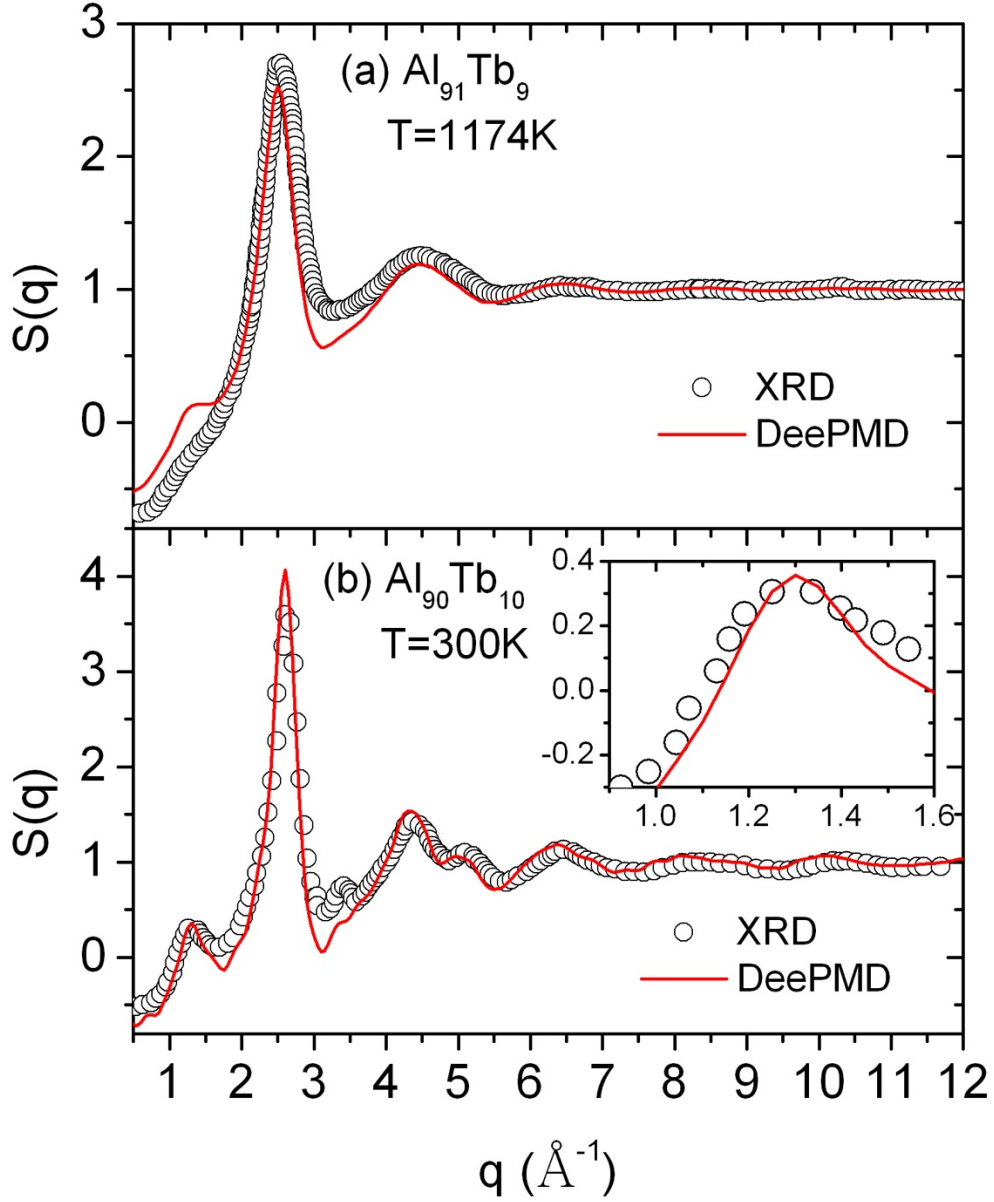


Fig. 8. The total structure factor of (a) liquid $\text{Al}_{91}\text{Tb}_9$ and (b) amorphous $\text{Al}_{90}\text{Tb}_{10}$ alloy. To obtain the amorphous $\text{Al}_{90}\text{Tb}_{10}$ for simulation, the sample is quenched from liquid at cooling rate of 10^{11} K/s. The inset figure shows the pre-peak (around 1.3 \AA^{-1}) of the total structure factor. It can be seen that the DeePMD well reproduces the position and height of the pre-peak.

- [1] A. Inoue, Prog. Mater. Sci. 43, 365 (1998).
- [2] Y. He, S. J. Poon, and G. J. Shiflet, Science 241, 1640 (1988).
- [3] H. S. Kim, P. J. Warren, B. Cantor, and H. R. Lee, Nanostruct. Mater. 11, 241 (1999).
- [4] Y. He, G. M. Dougherty, G. J. Shiflet, and S. J. Poon, Acta Metall. Mater. 41, 337 (1993).
- [5] A. L. Greer, Science 267, 1947 (1995).
- [6] J. C. Foley, D. R. Allen, and J. H. Perepezko, Scr. Mater. 35, 655 (1996).
- [7] Y. E. Kalay, L. S. Chumbley, and I. E. Anderson, Mater. Sci. Eng. A 490, 72 (2008).
- [8] A. Inoue, K. Ohtera, and T. Masumoto, Jpn. J. Appl. Phys. 27, L736 (1988).
- [9] M. I. Mendeleev, F. Zhang, Z. Ye, Y. Sun, M. C. Nguyen, S. R. Wilson, C. Z. Wang, and K. M. Ho, Modelling Simul. Mater. Sci. Eng. 23, 045013 (2015).
- [10] Feng Zhang, Yang Sun, Zhuo Ye, Yue Zhang, Cai-Zhuang Wang, Mikhail I Mendeleev, Ryan T Ott, Matthew J Kramer, Ze-Jun Ding, and Kai-Ming Ho, J. Phys.: Condens. Matter 27, 205701(2015).
- [11] Yang Sun, Yue Zhang, Feng Zhang, Zhuo Ye, Zejun Ding, Cai-Zhuang Wang, and Kai-Ming Ho, J. Appl. Phys. 120, 015901 (2016).
- [12] Linfeng Zhang, Jiequn Han, Han Wang, Roberto Car, and Weinan E, Phys. Rev. Lett. 120, 143001(2018).
- [13] Linfeng Zhang, Jiequn Han, Han Wang, Wissam A. Saidi, Roberto Car, and Weinan E, arXiv:1805.09003v2
- [14] Han Wang, Linfeng Zhang, Jiequn Han, and Weinan E, Computer Physics Communications 228, 178 (2018).
- [15] S. Plimpton, J. Comput. Phys. 117, 1 (1995).
- [16] G. Kresse and J. Furthmuller, Phys. Rev. B 54, 11169 (1996).
- [17] G. Kresse and J. Furthmuller, Comput. Mater. Sci. 6, 15 (1996).
- [18] S. Nose, J. Chem. Phys. 81, 511 (1984).
- [19] W. G. Hoover, Phys. Rev. A 31, 1695 (1985).
- [20] Y. E. Kalay, I. Kalay, Jinwoo Hwang, P. M. Voyles, M. J. Kramer, Acta Materialia 60, 994 (2012).
- [21] I. Pop, V. Crisan, M. Coldea, C. Hagan, and G. Borodi, Physica B+C 130, 504 (1985).
- [22] O. J. C. Runnalls and R. R. Boucher, J. Less-Common Met. 13, 431 (1967).
- [23] J. F. Cannon and H. Tracy Hall, J. Less-Common Met. 40, 313 (1975).
- [24] A. E. Dwight, J. Less-Common Met. 102, L9 (1984).
- [25] C Becle, R Lemaire, and E Parthe, Solid State Commun. 6, 115 (1968).
- [26] K. H. J. Buschow, J. Less-Common Met. 8, 209 (1965).
- [27] K. H. J. Buschow and A. S. Van Der Goot, J. Less-Common Met. 24, 117 (1971).
- [28] H. Haschke, H. Nowotny, and F. Benesovsky, Monatsh. Chem. 98, 273 (1967).
- [29] Vanderbilt D, Phys. Rev. B 41, 7892 (1990).
- [30] J. P. Perdew, K. Burke, and M. Ernzerhof, Phys. Rev. Lett. 77, 3865 (1996).
- [31] Tongqi Wen, Cai-Zhuang Wang, M. J. Kramer, Yang Sun, Beilin Ye, Haidi Wang, Xueyuan Liu, Chao Zhang, Feng Zhang, Kai-Ming Ho, and Nan Wang, Phys. Rev. B 100, 174101 (2019).
- [32] Anubhav Jain, Shyue Ping Ong, Geoffroy Hautier, Wei Chen, William Davidson

Richards, Stephen Dacek, Shreyas Cholia, Dan Gunter, David Skinner, Gerbrand Ceder, and Kristin A. Persson, *APL Materials* 1, 011002 (2013).

[33] D. M. Bailey, *Acta Cryst.* 23, 729(1967).

[34] F. Zhang, I. McBrearty, R. T. Ott, E. Park, M. I. Mendelev, M. J. Kramer, C. Z. Wang, and K. M. Ho, *Scr. Mater.* 81, 32 (2014).

[35] Z. Ye, F. Zhang, Y. Sun, M. I. Mendelev, R. T. Ott, E. Park, M. F. Besser, M. J. Kramer, Z. Ding, C.-Z. Wang, and K.-M. Ho, *Appl. Phys. Lett.* 106, 101903 (2015).